In-situ X-radiographic study of nucleation and growth behaviour of primary silicon particles during solidification of a hypereutectic Al-Si alloy

Yijiang Xu[a], Yun Deng[b], Daniele Casari[c], Ragnvald H. Mathiesen[c], Yanjun Li[a]*

a Department of Materials Science and Engineering, Norwegian University of Science and Technology (NTNU), N-7491 Trondheim, Norway

b Department of Mechanical and Industrial Engineering, Norwegian University of Science and Technology (NTNU), N-7491 Trondheim, Norway

c Department of Physics, Norwegian University of Science and Technology (NTNU), N-7491 Trondheim, Norway

*Corresponding Author. E-mail address: yanjun.li@ntnu.no (Y.J. Li)

Abstract:

Real-time observation of structure evolution in a hypereutectic Al-Si(-Cu) alloy under near-isothermal melt solidification condition was conducted by using in-situ micro-focus X-radiography. The nucleation, growth rate and morphological development of primary Si particles (PSPs) were studied at different cooling rates. It is found that an increase of cooling rate increases nucleation rate, reduces the crystal growth and extends the nucleation temperature range of primary Si particles, which all help to refine primary Si particles. The minimum nucleation undercooling also increases with increasing cooling rate. Based on the experimental findings, it is proposed that Si atom clusters act as the nuclei of Si crystals. In addition, cooling rate does not alter the branching growth mechanism of PSPs but only shorten the branch length and reduce the development of side plates. Higher cooling rate may increase the peak growth velocity of PSPs due to the higher nucleation undercooling. Further, electron backscatter diffraction (EBSD) characterization of the post solidified in-situ sample confirms that twinning in primary Si occurs in the nucleation stage or during the growth process, and the growth of twined branches and plates follows the twin plane re-entrant edge (TPRE) mechanism. Twinning during growth may facilitate the branching.

Key words: Hypereutectic Al-Si alloy; Primary Si particles; Nucleation; Crystal growth; Solidification; In-situ X-radiography

1. Introduction

The morphology and size of primary silicon particles (PSPs) have strong influences on the final mechanical properties of hypereutectic Al-Si alloys. Depending on the solidification conditions and alloy composition, a wide variety of morphologies with different sizes could form, such as

star-like, plate-like, polyhedral and feathery, etc., which is supposed to be controlled by its nucleation and growth behaviour [1, 2].

So far, experimental studies on nucleation and growth behaviour of PSPs have been mainly limited to thermal analysis during solidification [3-6], ex-situ characterization of the size and morphology of PSPs by optical microscope (OM), scanning electron microscope (SEM) and X-ray tomography [3, 5, 7-22]. In addition, crystallographic investigations have been carried out by electron backscatter diffraction (EBSD) and transmission electron microscopy (TEM) [21, 23, 24]. 2D morphologies were commonly observed by OM and SEM on the surface of the cast sample, while quasi-3D morphologies were observed via SEM after deep etching. Twin plane re-entrant edge (TPRE) growth mechanism was proposed for the growth of plate-like and five-fold twined primary Si particles through crystallography and morphology analysis [8, 25]. Besides, for the spinel twinned octahedra, Wang et al. [26-28] proposed the dislocation emerging and accelerated corner growth mechanism by observing etched growth steps on the polished cross section of Si particles. Recently, 3D morphologies of octahedral and spinel shaped primary Si particles have been visualized by synchrotron X-ray tomography in hypereutectic Al-Si samples produced by permanent-mold casting [19-21], by which the growth speed ratios between different crystalline directions were deduced. Xu et al. [12] investigated the size and morphology of PSPs cast in copper molds at different cooling rates from 90 K/s to 1.16×10^6 K/s by SEM. It was found that the size of primary silicon decreased gradually with increasing cooling rate, while significant morphology change only occurred under extremely rapid solidification conditions. Bridgman directional solidification experiments [9] showed that the morphology of primary silicon changes from plate-like to polyhedral with increase of equivalent cooling rate (product of pulling velocity and temperature gradient), but the estimated nucleation undercooling was found to be independent of the solidification conditions. In addition, droplet emulsion experiments [29] showed that the morphology largely depends on the undercooling, which influences both nucleation and growth of primary silicon. However, direct measurement of nucleation undercooling of PSPs is difficult.

There has been a few attempts on in-situ study of nucleation and growth of PSPs. Kasprzak et al. [30] carried out an in-situ neutron diffraction study on the solidification of a hypereutectic Al-Si alloy, by which the nucleation starting temperature and the volume fraction evolution of primary Si were measured. The detection of diffraction intensity peak of Si above the thermodynamic liquidus temperature indicated the existence of Si atom clusters before

precipitation of Si crystals, which is in agreement with other investigations from small angle neutron scattering [31]. However, it is not possible to track the nucleation and growth kinetics of individual PSPs with this technique. Mao et al. [32] utilized in-situ synchrotron X-ray radiography to observe the nucleation and growth behaviour of PSPs in a Zn based alloy, Zn-27Al-3Si under the influence of Sr modification. It shows that Sr modification has the influence of suppressing the nucleation of PSPs while increasing their growth rate. However, the morphology of PSPs in this alloy is different from those in Al-Si hypereutectic alloys. Shahani et al. [33] studied the interfacial growth dynamics of silicon particles in an Al-32Si-15Cu alloy at very low cooling rate by in-situ synchrotron X-ray tomography. This study mainly focuses on the twin related crystal growth but not on the growth morphology and growth velocity. The habit plane and grain boundary during growth were quantified through analysis of the normal direction of the interface. Crystal growth with twining was observed.

Quantitative experimental study on the nucleation and growth kinetics of PSPs in hypereutectic Al-Si alloys, is still missing. In this work, for the first time, in-situ micro-focus X-radiography has been applied to study the nucleation and growth kinetics of PSPs during solidification of a high-purity hypereutectic Al-Si-Cu alloy. The advantage with this setup, compared to the synchrotron X-ray radiography and tomography, is that floating of Si crystals can be avoided during solidification by proper alignment of the thin radiography cell with respect to gravity. The solidified thin samples are further studied by ex-situ characterization using SEM and EBSD.

2. Experimental

The material used in this study is an Al-22wt.%Si-18.8wt.%Cu alloy, prepared by melting 5N high-purity aluminium, 6N high-purity Si and 6N high-purity Cu in a clay graphite crucible using a Nabertherm melting furnace. After complete melting and mixing of the raw materials, the melt was cast into a copper mould. Afterwards, plate-like thin samples were first cut from the solidified ingot then ground and polished into the final dimension of 5*50*0.2(X*Y*Z) ±0.01 mm. Measured by Glow Discharge Mass Spectrometry (GDMS), the phosphorus content in the alloy is only 0.47 ppm, which is extremely low. The aim of adding Cu is to enhance the X-radiography contrast between primary Si phase and liquid phase, similar to the approach employed by Mathiesen et al. [34] to study eutectic Al-Si solidification. The liquidus temperature of the present alloy calculated by Thermo-Calc [35] using the TCAL4 database is

770.2 ^{o}C (point #1 in the phase diagram provided in the Appendix), at which primary Si can start to form during solidification.

The in-situ microfocus X-radiography experiments were carried out at the home laboratory, where the setup has been widely used for observing primary Al grains (equiaxed and elongated dendrites), eutectic transformations, α-Al(FeMnCr)Si intermetallics in Al alloys [36-40] and α-Mg dendrites in Mg alloys [41]. A detailed description of the whole set-up could be found in Ref. [39]. In the present study, a fine focus power setting of 50 kV and 55 μA was employed for the X-ray source using molybdenum as the target material. The image recording rate of the CCD camera is 1 frame per second. The size of the field-of-view (FOV) is about 2700*1800 μm^2 (1.34 μm/pixel).

Thin plate samples encapsulated by glassy carbon crucibles were melted and solidified inside the Gradient Furnace in a horizontal position, namely, the wide surface of the sample X-Y plane is perpendicular to the gravity direction. By this configuration, melt convection can to a large extent be reduced and crystal movement due to gravity/flotation is limited. Thus, it simplifies the condition for studying the nucleation and growth kinetics of primary silicon. The initial melt temperature is ~790 ^{o}C. Near-isothermal melt solidification with constant cooling rates in the range of 0.05-1 K/s were applied by controlled power-down of the two heater elements simultaneously.

After the last sequence of in-situ solidification experiments, an area including the in-situ FOV were cut out from the thin sample and then ground with grit 4000 SiC paper, polished with 3 and 1 μm diamond paste followed by a final polishing with 0.25 μm oxide polishing suspension. The microstructure was examined via secondary electron imaging (SEI) and electron back-scattered diffraction (EBSD) using a FEI Quanta 650 FEG scanning electron microscopy (SEM) equipped with a NORDIF EBSD detector and TSL OIM software. The operating conditions of EBSD scanning were as follows: accelerating voltage 20 kV, sample tilt 70°, working distance 12.5 mm and step size 1-4 μm.

3. Results

3.1. In-situ observation

The in-situ X-radiography image sequences recorded during near-isothermal melt solidification of high-purity hypereutectic Al-22Si-18.8Cu alloy under three different cooling rates, 0.2, 0.5 and 1 K/s, are shown in Fig. 1. In each solidification sequence, when the first Si

particle becomes visible in the FOV, the time is set to t=0 s. The melt temperature is obtained from the thermocouples calibrated with the temperature of Al dendrites forming in the FOV (assuming Al forms at the theoretical binary Al-Si eutectic temperature of this ternary alloy, T=528.9 ^{o}C, as shown by point #2 in the Al-18.8Cu-xSi phase diagram calculated by Thermo-Calc [35] in the Appendix). Due to the difference of Cu concentration between the liquid and solid phases, primary Si crystals forming in the liquid (some are indicated by the red arrows) show a bright contrast while the liquid remains dark. It was found that some porosity formed in the samples already in the initial melting, and these pores were sometimes found difficult to remove. Thus, the pores will also form bright contrast features in the raw transmission images. To have visible image contrast, flat field corrections of the raw images are required, and the flat fields are prepared from a few images taken through the sample with a homogeneous melt. As the pores move around in the liquid during the solidification process (e.g. by thermal contraction), traces of pores turn out as black spots in the flat field corrected images, as marked by the blue arrows in Fig. 1.

As can be seen in Fig. 1, PSPs precipitate nearly uniformly in the whole FOV. After nucleation, a faceted growth of PSPs can be seen and quasi-3D morphologies of PSPs during solidification can be captured. Most of the PSPs show complex star-like morphologies with branches and fan-like thin plates extending into the surrounding Al liquid. With temperature decreasing, elongated branches and side plates grow into larger sizes. Formation of new plates on the growing branches can also be seen (e.g. L2_A in Fig. 1a). For particles forming at higher cooling rates, orthogonal branches (marked by the yellow arrow) are often observed, which is very similar to the imperfect or hopper octahedron primary Si in the non-inoculated hypereutectic Al-Si alloy forming under fast cooling conditions observed by SEM [13]. Besides, the branches and side plates of PSPs become less extended, and the size of PSPs decreases as cooling rate is further increased.

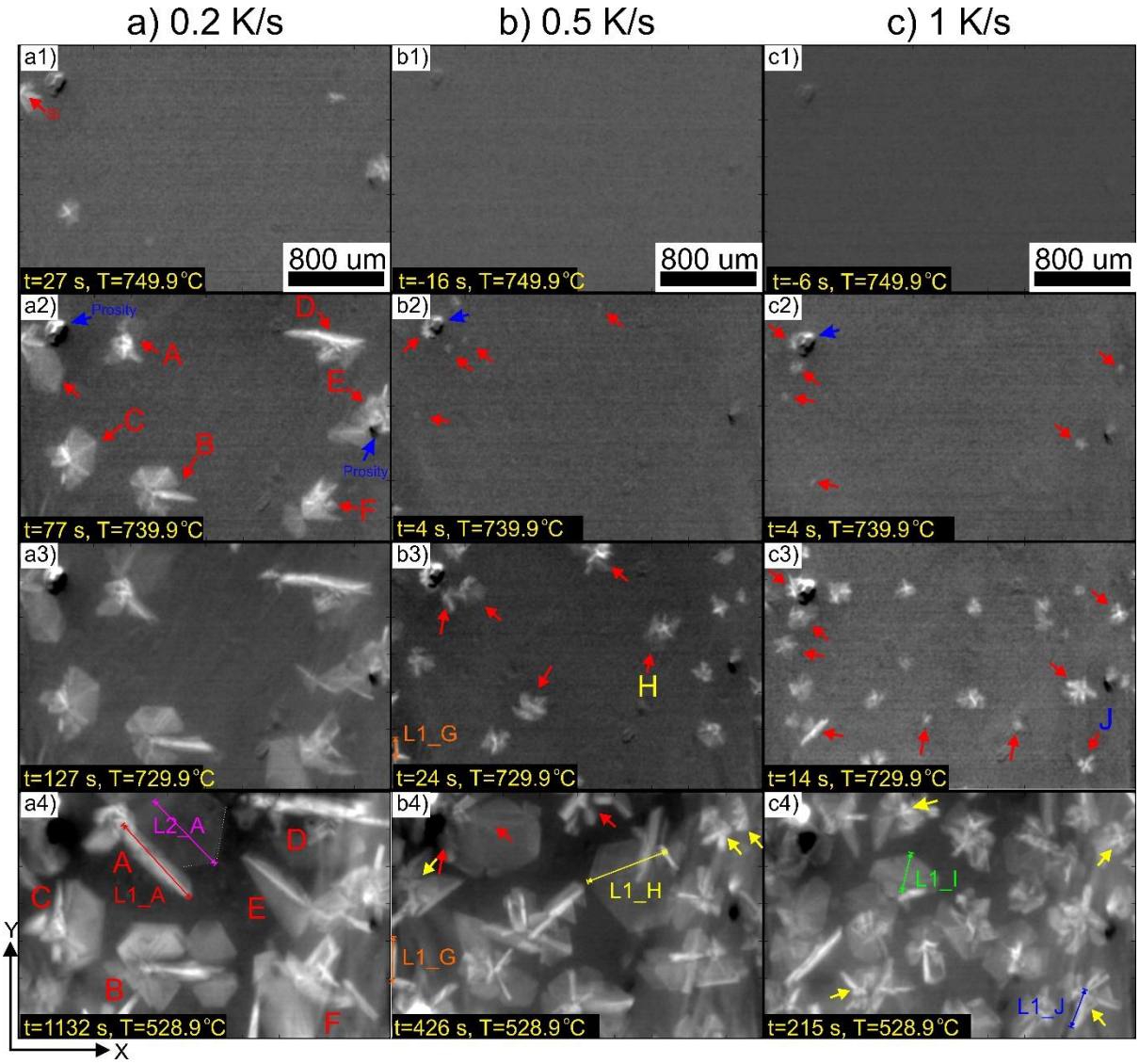

Fig. 1. Selected X-radiographic images from in-situ solidification experiments of high-purity hypereutectic Al-Si(-Cu) alloy under three different cooling rates, (a) 0.2, (b) 0.5 and (c)1 K/s, respectively. The solidification time t and melt temperature T are marked in each image.

3.2. Nucleation kinetics

Fig. 2a shows the evolution of the total number of primary Si particles formed in the FOV at five different cooling rates (including the three solidification scenarios illustrated in Fig. 1) as a function of undercooling until the nucleation process ends. As can be seen, primary Si starts to nucleate at different undercoolings dependent of cooling rate, ranging from 14.4 K to 28.3 K. As a general trend, the minimum undercooling required for nucleation of primary Si increases with cooling rate. The total number of PSPs increases with decreasing temperature until nucleation ceases. It is interesting to see that the number of PSPs shows a nearly linear relationship with undercooling, while the slope increases with cooling rate. Fig.2b shows the

final volumetric number density of PSPs as a function of cooling rate. As can be seen, a higher cooling rate promotes nucleation of PSPs.

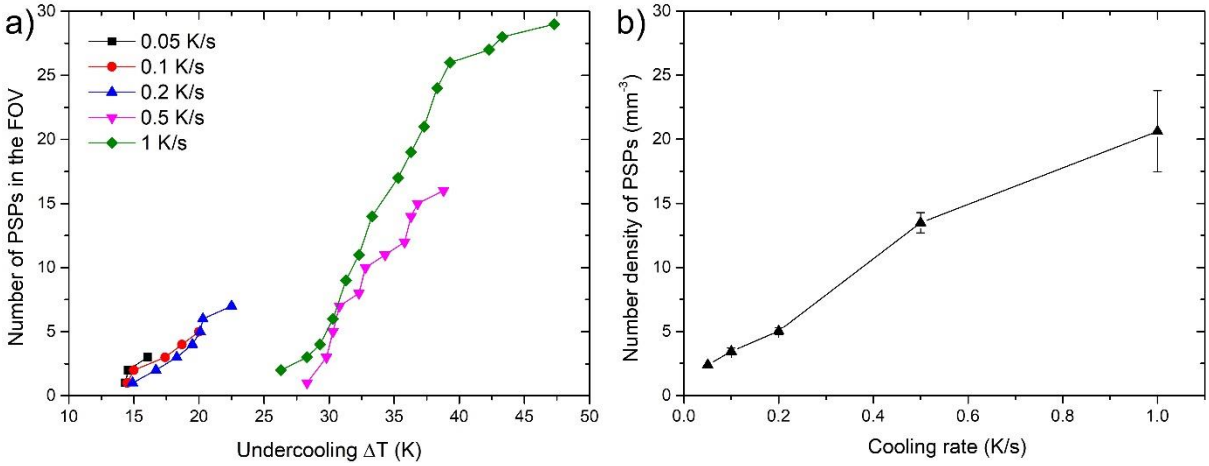

Fig. 2. The evolution of total number of PSPs in the FOV as a function of undercooling for 5 different cooling rates (including the solidification cases shown in Fig. 1). (b) Final number density of PSPs as a function of cooling rate.

The measured minimum nucleation undercooling (undercooling below the liquidus temperature when nucleation starts), and maximum nucleation undercooling (undercooling below the liquidus temperature when nucleation stops), as a function of cooling rate in the range of 0.05-1 K/s, are shown in Fig. 3. Evidently, both the minimum and maximum nucleation undercooling increase with cooling rate. The temperature range for nucleation of PSPs also increases with increasing cooling rate.

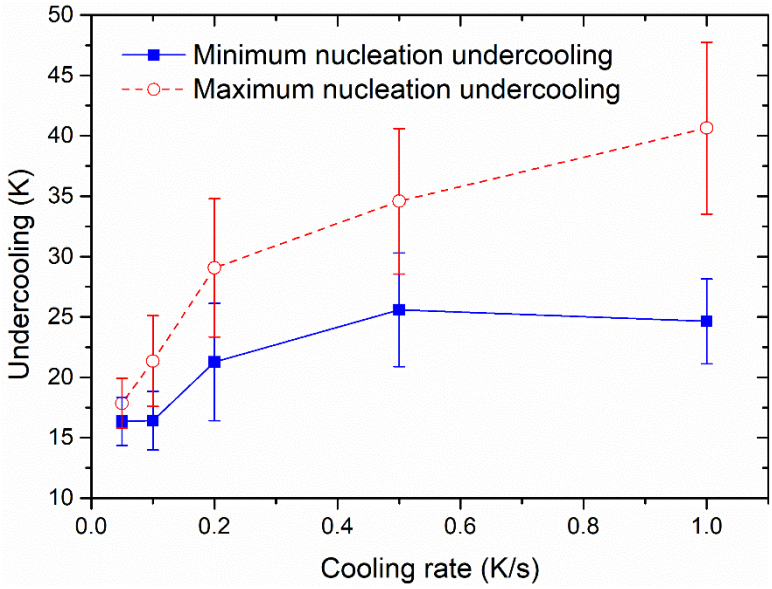

Fig. 3. Minimum nucleation undercooling and maximum nucleation undercooling of PSPs measured from in-situ solidification experiments of high-purity hypereutectic Al-Si(-Cu) alloy

as a function of cooling rate. The error bars indicate the standard deviation of the experimental data measured for different solidification experiments.

3.3. Growth kinetics

The growth of selected PSPs in Fig.1 has been analysed through tracking the length development of branches and side plates as a function of solidification time/temperature. As illustrated in Fig. 1, the length is measured from the nucleation centre of the primary Si particles. Representative measurements from 3 different cooling rates are plotted in Fig. 4a (branches) and Fig. 4b (plates), respectively. Apparently, the cooling rate significantly affects the growth kinetics of Si particles, both elongated branches and side plates. At low cooling rates, the growth of Si particles can proceed within a longer time to a higher length over the same temperature range, especially at high temperatures. As the cooling rate increases, the growth of Si particle is reduced greatly, ending up with a smaller final particle size.

The growth velocity obtained from the first derivative of growth curves (length as a function of time) are shown in Fig. 4c and Fig. 4d. As can be seen, for branch L1 of particle J and plate L2 of particle A, there is an increase of the growth velocity in the initial stage and followed with a decreasing after reaching a peak value. For other particles, the growth velocity already starts to decrease in the initial stage been detected. In the late solidification stage below 640 ^{o}C, the growth velocity of all particles is very small, mostly below1 μm/s.

If we compare the growth of different branches and side plates, a general trend can be observed: the peak growth velocity of the Si crystals increases with nucleation undercooling, which also increases with cooling rate. Moreover, at the same melt temperature above 680 ^{o}C (thus same undercooling), the growth velocity varies between different branches/plates, indicating that there are other factors influencing the growth kinetics of facetted PSPs. Besides, it can be seen that the growth velocity at low temperature below 640 ^{o}C is quite similar and largely independent of cooling rate.

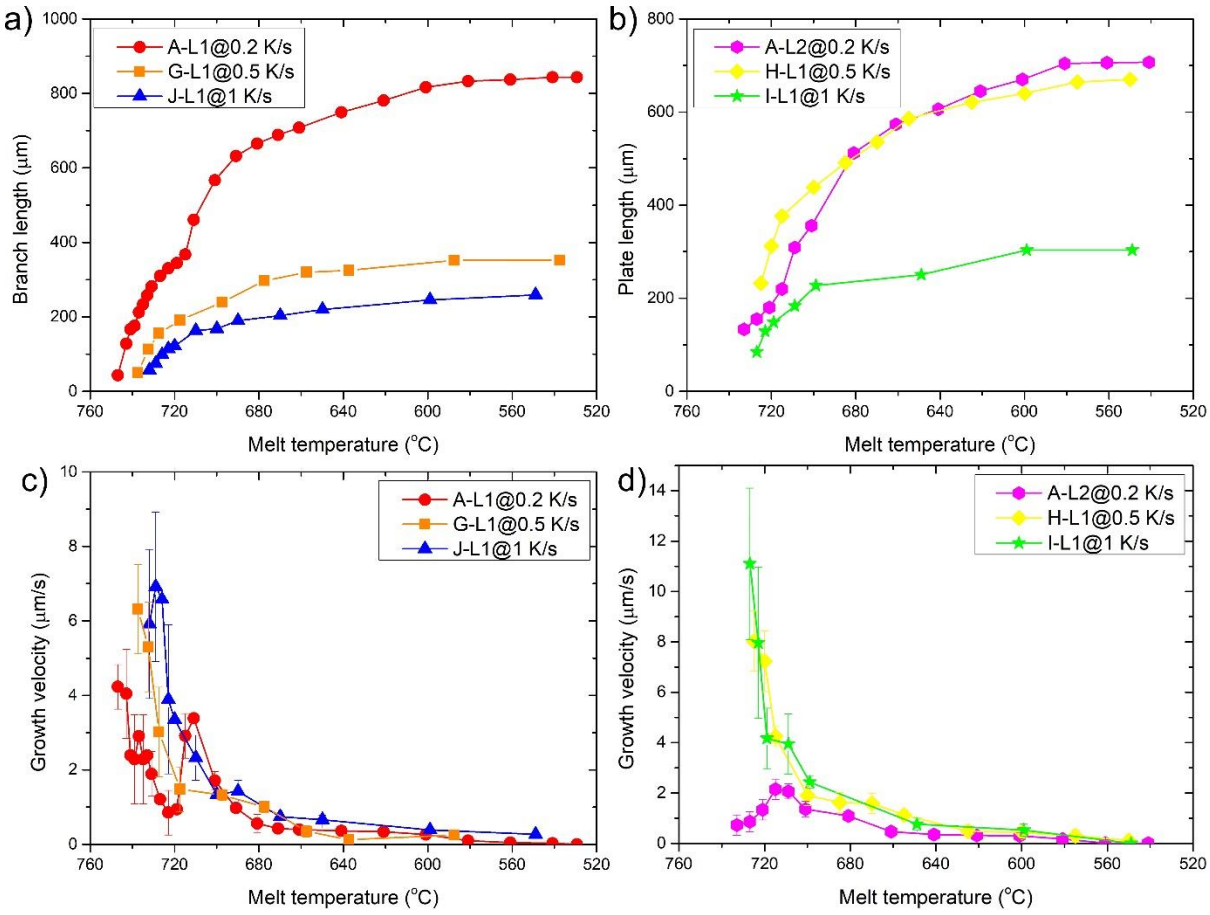

Fig. 4. (a) (b) Evolution of individual branches (a) and plates (b) of the primary Si marked and shown in Fig.1 as a function of melt temperature during solidification at 3 different cooling rates. (c) (d) Measured growth velocity of the corresponding primary Si particles shown in (a) and (b) in unite of μm/s.

3.4. Ex-situ characterization of post-solidified sample

Fig. 5a shows the final solidification microstructure of PSPs from the 0.2 K/s sequence illustrated in Fig. 1a, taken at T= 528.7 ºC just before the Al-Si eutectic starts forming. Fig. 5b shows a secondary electron (SE) image of the same sample region from the post-solidified sample. It is noteworthy that SE image only shows the 2D morphology of primary Si particles in the polished sample surface, which looks different from the quasi-3D morphology in the in-situ projection image. After polishing, the large broad plate in particle A becomes a narrower plate. Some part of particle B and particle C disappear in the 2D cross section, which is due to the mechanical polishing. Besides, a triangular pyramid in particle E cannot be observed in the SE image. It clearly shows the advantage of in-situ X-radiography in revealing the morphology and growth kinetics of primary Si particles during solidification.

Fig. 5c and 5d display the EBSD orientation map and the {111} pole figures, respectively, for some of the primary Si particles in Fig. 5a and Fig. 5b. As can be seen, all the primary Si particles are multi-crystalline, containing {111} twin boundaries (TB, as marked by the black lines). For particle A, the big plate has a twin orientation relationship with the pink crystal in branch L1 and L3. In the in-situ X-radiographic images, the plate is connected to L1. Besides, the branch L1 also consists of two twin crystals (blue and pink colour), and the length direction is parallel to the twin boundary trace, indicating that the growth of Si crystals is mainly based on the twin plane re-entrant edge (TPRE) mechanism. Twin orientation relationships between different parts of branches and plates can also be observed in particles B and C. There are three twin orientation relationships between four different crystals in particle B. Particle D has multiple twinning along the growth direction. The edge-on cross sections of branches in particle B and D also show the TPRE growth.

According to the in-situ X-radiographic video, starting points of the PSPs are assumed to be the nucleation centres, which are marked on the EBSD images with red circular dots. For most of the particles characterized by EBSD, many twin boundaries are found to initiate from the nucleation centre, implying that these nuclei may originally contain several twin crystals. Besides, some twin boundaries are far away from the nucleation centre (as indicated by the arrows in side plate P2 of particle A, particle B and particle C). These twin boundaries are usually found in the new side branches and plates forming in the later stage of crystal growth, which also have twin orientation relationships with initial crystals of the nuclei. With the formation of new branches and side plate crystals, the morphology of Si particles becomes more complex, e.g., particle B, which can be clearly seen from the in-situ image sequences. One can also find that for all the side branches of Si crystals, their elongation directions are parallel to the twin boundary traces, confirming the TPRE growth mechanism of PSPs.

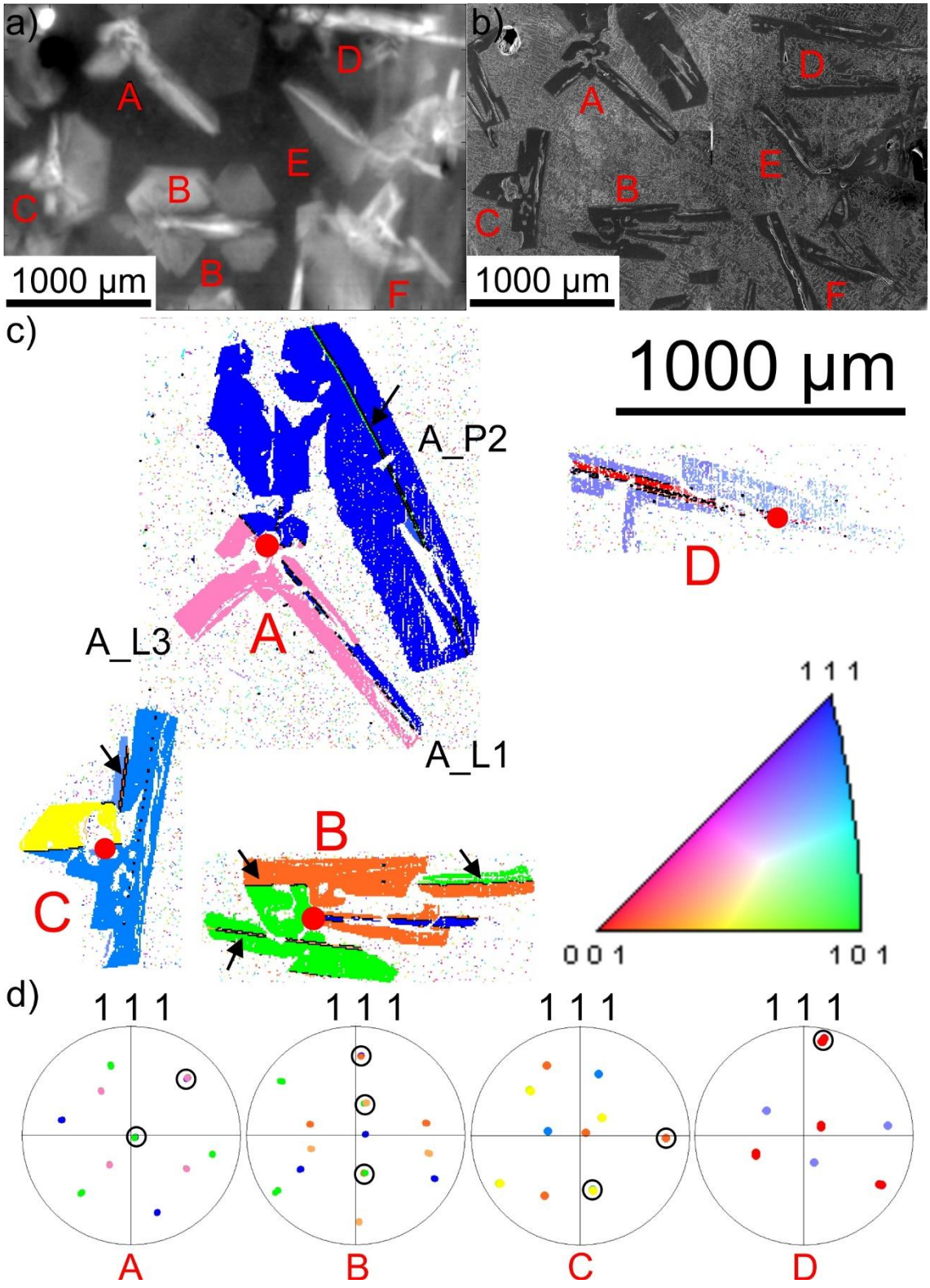

Fig. 5. (a) Primary silicon particles recorded by in-situ X-radiography before Al forming during solidification of the hypereutectic Al-Si(-Cu) alloy at 0.2 K/s. (b) Secondary electron image of the post-solidification structure of the in-situ X-radiography sample shown in (a). (c) EBSD orientation map of some primary Si particles where twin boundaries are marked with black lines. Separated maps were taken on each particle. (d) The {111} pole figures of the corresponding crystals in the twinned primary Si particles.

4. Discussion

As can be seen from Fig. 1-Fig. 3, the nucleation kinetics of primary Si particles in the present hypereutectic Al-Si(-Cu) alloy is significantly influenced by cooling rate. Because the phosphorus content in the alloy is only 0.47 ppm, it can be considered that there are no AlP particles forming in the melt. Previously reported experimental results [5, 30, 31] show that Si-Si atom clusters exist in the melt even above the liquidus temperature. Fig. 3 shows that the minimum nucleation undercooling of PSPs increases with cooling rate. This can be attributed to the cooling rate dependent evolution of Si-Si atom clusters in the liquid metal during solidification. According to the classical nucleation theory [42], Si-Si atom clusters (embryos) form in the melt due to concentration fluctuations. The equilibrium size distribution of clusters is dependent of the undercooling. The number of the clusters with sizes equal to or larger than the critical radius of nucleus increases with undercooling. However, solidification is a non-equilibrium process, for low undercooling, the formation of such large atom clusters has to be through diffusion-controlled growth and coarsening processes. At slow cooling rate, Si atom clusters have more time to grow into effective nuclei of Si crystals. Therefore, the minimum undercooling needed for nucleation of PSPs is smaller. However, at small undercooling the number of effective nuclei is also small. Once Si crystals grow from the nuclei, the supersaturated Si content in the surrounding liquid will be quickly consumed, making the nucleation of new Si particles difficult. As a result, the number density of PSPs is low while the size of PSPs is large. On the contrary, at higher cooling rates, Si atom clusters have less time to grow thus more clusters with smaller size survive. So, the minimum nucleation undercooling of PSPs is larger and the nucleation rate is enhanced. In addition, the PSPs have less time to grow and therefore the solute segregation stifling effect is weaker under higher cooling rates. As a result, the undercooling range for nucleation is extended (Fig. 3) and more clusters can reach the critical size and be activated for nucleation of Si particles. All of these explain the promotion effect of high cooling rate on the nucleation and refinement of PSPs and the different nucleation behaviours shown in Fig. 1-Fig. 3.

Moreover, an increase of cooling rate from 0.2 to 1.0 K/s seems not to alter the growth morphology and branching growth mechanism of PSPs, but only shorten the branch length and reduce the development of side plates. As reported in Ref. [12], a super-high cooling rate is necessary to change the morphology of PSPs in non-inoculated/unmodified hypereutectic Al-Si alloys. For the growth kinetics, cooling rate mainly influence the peak growth velocity indirectly by influencing the nucleation undercooling of PSPs. But, in the later stage, the

growth of PSPs might be influenced by many factors, such as solute impingement [43] by surrounding growing Si crystals, crystallographic growth direction and surface defects [44] etc..

Due to the low stacking fault energy of Si (low grain boundary energy of Σ3{111} TB, 0.014 J/m^2 [45, 46]), twins are commonly observed in Si crystals after solidification, either pure Si, eutectic Si or primary Si. There has been much debate on when and where such twins form, i.e., whether the critical nucleus originally contains a twin boundary [26, 27, 47] or whether the twin boundaries form after nucleation [48-50]. Through combined in-situ observation and ex-situ EBSD characterization of the PSPs in the present work, it is found that twins form in both the nucleation and growth stages. From the observation in particle B and C that new side branches and plates always contain twins, it can be proposed that twinning during growth may facilitate the branching. Besides, by analyzing the twin boundary traces and edge-on cross sections, it is confirmed that the growth of twinned PSPs is based on the twin plane re-entrant edge (TPRE) mechanism.

5. Conclusions

Nucleation and growth behaviour of primary silicon particles (PSPs) during isothermal melt solidification of a non-inoculated/unmodified hypereutectic Al-Si(-Cu) alloy have been studied via in-situ X-radiography and ex-situ EBSD characterization. The main findings are:

Higher cooling rate enhances the nucleation rate and increases the final number density of PSPs. Higher cooling rate also extends the temperature range for nucleation of PSPs although both the minimum and maximum nucleation undercooling increase with increasing cooling rate. The minimum nucleation undercooling is in the range of 14.4-28.3 K. Based on the in-situ experimental results, it is also proposed that Si atom clusters have acted as the nucleation site of primary Si particles.

The cooling rates studied here do not change the branching growth mechanism and growth morphology of PSPs. But higher cooling rate results in smaller size and more compact shapes, of which the branches become shorter and the side pates are less developed. The peak growth velocity of PSPs increases with increasing cooling rate, due to the increase of nucleation undercooling.

By further ex-situ EBSD characterization of PSPs formed during in-situ experiments, it is revealed that twin plane re-entrant edge mechanism is the dominating growth mechanism for

primary Si. In addition, twin boundaries can form both in the initial nucleation stage and in the later growth process.

Acknowledgments

The financial support by The Research Council of Norway (PRIMARL Project, Grant number: 236675) and industrial partners Hydro Aluminium and Alcoa (Norway) is greatly acknowledged.

Appendix

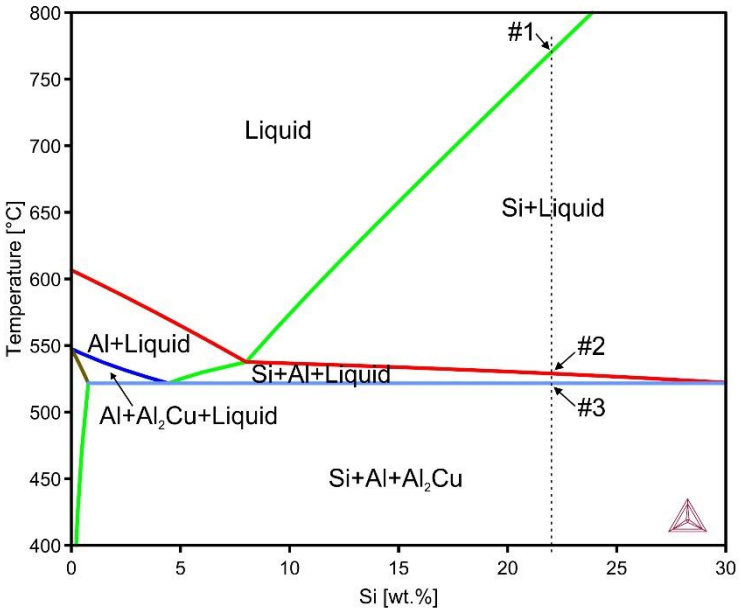

Fig. A1. Phase diagram of Al-18.8Cu-xSi calculated by Thermo-Calc. #1 represents the liquidus temperature (770.2 ^{o}C) below which primary Si forms, #2 represents Al-Si binary eutectic temperature (528.9 ^{o}C) and #3 represents Al-Si-Al2Cu ternary eutectic point (521.6 ^{o}C).

References

[1] J.E. Gruzleski, Hypereutectic Aluminium-Silicon Casting Alloys—A Review AU - Tenekedjiev, N, Cast Metals, 3 (1990) 96-105.
[2] V. V, K. Narayan Prabhu, Review of Microstructure Evolution in Hypereutectic Al–Si Alloys and its Effect on Wear Properties, Transactions of the Indian Institute of Metals, 67 (2014) 1-18.
[3] Y. Liu, Y. Zhang, W. Yu, X. Wang, H. Zheng, X. Tian, Pre-nucleation clusters mediated crystallization in Al–Si melts, Scripta Materialia, 110 (2016) 87-91.
[4] W. Yu, Y. Zhang, A. Jiang, T. Yan, Y. Tian, H. Zheng, X. Lin, X. Tian, Promoted nucleation of potent substrates assisted with Al-10Si-2Fe master alloy in Al-Si alloys, Materials Letters, 207 (2017) 93-95.

[5] W. Wang, X. Bian, J. Qin, S.I. Syliusarenko, The atomic-structure changes in Al-16 pct Si alloy above the liquidus, Metallurgical and Materials Transactions A, 31 (2000) 2163-2168.
[6] W. Yu, Y. Zhang, T. Yan, Y. Liu, A. Jiang, H. Zheng, X. Tian, Enhanced nucleation of primary silicon in Al-20 wt. % Si alloy with Ni-Si inoculation, Journal of Alloys and Compounds, 693 (2017) 303-307.
[7] H. Fredriksson, M. Hillert, N. Lange, The modification of aluminum-silicon alloys by sodium, J. Inst. Met., 101 (1973) 285-299.
[8] K. Kobayashi, L.M. Hogan, Fivefold twinned silicon crystals grown in an A1–16 wt.% Si melt, Philosophical Magazine A, 40 (1979) 399-407.
[9] D. Liang, Y. Bayraktar, H. Jones, Formation and segregation of primary silicon in Bridgman solidified Al-18.3 wt% Si alloy, Acta Metallurgica et Materialia, 43 (1995) 579-585.
[10] Z.-h. Zhang, X.-f. Bian, Y. WANG, X. Liu, Refinement and thermal analysis of hypereutectic Al-25% Si alloy, J TRANSACTIONS-NONFERROUS METALS SOCIETY OF CHINA-ENGLISH EDITION, 11 (2001) 374-377.
[11] G.I. Eskin, D.G. Eskin, Some control mechanisms of spatial solidification in light alloys, Zeitschrift für Metallkunde, 95 (2004) 682-690.
[12] C.L. Xu, Q.C. Jiang, Morphologies of primary silicon in hypereutectic Al–Si alloys with melt overheating temperature and cooling rate, Materials Science and Engineering: A, 437 (2006) 451-455.
[13] C.L. Xu, H.Y. Wang, C. Liu, Q.C. Jiang, Growth of octahedral primary silicon in cast hypereutectic Al–Si alloys, Journal of Crystal Growth, 291 (2006) 540-547.
[14] H. Yamagata, W. Kasprzak, M. Aniolek, H. Kurita, J.H. Sokolowski, The effect of average cooling rates on the microstructure of the Al–20% Si high pressure die casting alloy used for monolithic cylinder blocks, Journal of Materials Processing Technology, 203 (2008) 333-341.
[15] H. Singh, A.M. Gokhale, A. Tewari, S. Zhang, Y. Mao, Three-dimensional visualization and quantitative characterization of primary silicon particles in an Al–Si base alloy, Scripta Materialia, 61 (2009) 441-444.
[16] Y. Zhang, H. Zheng, Y. Liu, R. Xu, L. Shi, X. Tian, Enhanced nucleation of primary silicon in Al–20Si (wt%) alloy inoculated with Al–10Si–2Fe master alloy, Materials Letters, 123 (2014) 224-228.
[17] J. Li, F.S. Hage, X. Liu, Q. Ramasse, P. Schumacher, Revealing heterogeneous nucleation of primary Si and eutectic Si by AlP in hypereutectic Al-Si alloys, Scientific Reports, 6 (2016) 25244.
[18] X. Chen, Y. Zhong, T. Zheng, Z. Shen, J. Wang, L. Fan, Y. Zhai, M. Peng, B. Zhou, W. Ren, Z. Lei, Z. Ren, Q. He, Refinement of primary Si in the bulk solidified Al-20 wt.%Si alloy assisting by high static magnetic field and phosphorus addition, Journal of Alloys and Compounds, 714 (2017) 39-46.
[19] J. Wang, Z. Guo, J.L. Song, W.X. Hu, J.C. Li, S.M. Xiong, Morphology transition of the primary silicon particles in a hypereutectic A390 alloy in high pressure die casting, Scientific Reports, 7 (2017) 14994.
[20] J. Wang, Z. Guo, S.M. Xiong, Characterization of the morphology of primary silicon particles using synchrotron X-ray tomography, Materials Characterization, 123 (2017) 354-359.
[21] J. Wang, Z. Guo, J.L. Song, W.X. Hu, J.C. Li, S.M. Xiong, On the growth mechanism of the primary silicon particle in a hypereutectic Al-20wt%Si alloy using synchrotron X-ray tomography, Materials & Design, 137 (2018) 176-183.

[22] J. Nie, Y. Zhao, Y. Li, F. Wang, H. Yang, K. Hu, G. Liu, X. Liu, Reactive synthesis of hexagonal Ti5P3.16 crystals and their heterogenous nucleating mechanism on primary Si, Journal of Alloys and Compounds, 777 (2019) 8-17.
[23] Y.T. Pei, J.T.M. De Hosson, Five-fold branched Si particles in laser clad AlSi functionally graded materials, Acta Materialia, 49 (2001) 561-571.
[24] M. Kim, Electron back scattering diffraction (EBSD) analysis of hypereutectic Al−Si alloys modified by Sr and Sc, Metals and Materials International, 13 (2007) 103.
[25] K. Kobayashi, P.H. Shingu, R. Ozaki, Crystal growth of the primary silicon in an Al-16 wt % Si alloy, Journal of Materials Science, 10 (1975) 290-299.
[26] R.-y. Wang, W.-h. Lu, L.M. Hogan, Twin related silicon crystals in Al–Si alloys and their growth mechanism, Materials Science and Technology, 11 (1995) 441-449.
[27] R.-Y. Wang, W.-H. Lu, L.M. Hogan, Faceted growth of silicon crystals in Al-Si alloys, Metallurgical and Materials Transactions A, 28 (1997) 1233-1243.
[28] R.-y. Wang, W.-h. Lu, L.M. Hogan, Growth morphology of primary silicon in cast Al–Si alloys and the mechanism of concentric growth, Journal of Crystal Growth, 207 (1999) 43-54.
[29] H.S. Kang, W.Y. Yoon, K.H. Kim, M.H. Kim, Y.P. Yoon, Microstructure selections in the undercooled hypereutectic Al–Si alloys, Materials Science and Engineering: A, 404 (2005) 117-123.
[30] W. Kasprzak, D. Sediako, M. Walker, M. Sahoo, I. Swainson, Solidification Analysis of an Al-19 Pct Si Alloy Using In-Situ Neutron Diffraction, Metallurgical and Materials Transactions A, 42 (2011) 1854-1862.
[31] M. Calvo-Dahlborg, P.S. Popel, M.J. Kramer, M. Besser, J.R. Morris, U. Dahlborg, Superheat-dependent microstructure of molten Al–Si alloys of different compositions studied by small angle neutron scattering, Journal of Alloys and Compounds, 550 (2013) 9-22.
[32] F. Mao, F. Chen, Q. Han, J. Han, Z. Cao, T. Wang, T. Li, Real time observation on the solidification of strontium-modified zinc–aluminum–silicon alloys by synchrotron microradiography, Journal of Alloys and Compounds, 608 (2014) 343-351.
[33] A.J. Shahani, E.B. Gulsoy, S.O. Poulsen, X. Xiao, P.W. Voorhees, Twin-mediated crystal growth: an enigma resolved, Scientific Reports, 6 (2016) 28651.
[34] R.H. Mathiesen, L. Arnberg, Y. Li, V. Meier, P.L. Schaffer, I. Snigireva, A. Snigirev, A.K. Dahle, X-Ray Videomicroscopy Studies of Eutectic Al-Si Solidification in Al-Si-Cu, Metallurgical and Materials Transactions A, 42 (2011) 170-180.
[35] https://www.thermocalc.com/, in.
[36] A.G. Murphy, W.U. Mirihanage, D.J. Browne, R.H. Mathiesen, Equiaxed dendritic solidification and grain refiner potency characterised through in situ X-radiography, Acta Materialia, 95 (2015) 83-89.
[37] Y. Xu, D. Casari, Q. Du, R.H. Mathiesen, L. Arnberg, Y. Li, Heterogeneous nucleation and grain growth of inoculated aluminium alloys: An integrated study by in-situ X-radiography and numerical modelling, Acta Materialia, 140 (2017) 224-239.
[38] Y. Xu, D. Casari, R.H. Mathiesen, Y. Li, Revealing the heterogeneous nucleation behavior of equiaxed grains of inoculated Al alloys during directional solidification, Acta Materialia, 149 (2018) 312-325.
[39] A.G. Murphy, D.J. Browne, W.U. Mirihanage, R.H. Mathiesen, Combined in situ X-ray radiographic observations and post-solidification metallographic characterisation of eutectic transformations in Al–Cu alloy systems, Acta Materialia, 61 (2013) 4559-4571.
[40] A. Bjurenstedt, D. Casari, S. Seifeddine, R.H. Mathiesen, A.K. Dahle, In-situ study of morphology and growth of primary α-Al(FeMnCr)Si intermetallics in an Al-Si alloy, Acta Materialia, 130 (2017) 1-9.

[41] D. Casari, W.U. Mirihanage, K.V. Falch, I.G. Ringdalen, J. Friis, R. Schmid-Fetzer, D. Zhao, Y. Li, W.H. Sillekens, R.H. Mathiesen, α-Mg primary phase formation and dendritic morphology transition in solidification of a Mg-Nd-Gd-Zn-Zr casting alloy, Acta Materialia, 116 (2016) 177-187.
[42] W. Kurz, D.J. Fisher, Fundamentals of Solidification, 4th ed., Trans Tech Publication LTD, 1998.
[43] D.A. Porter, K.E. Easterling, M. Sherif, Phase Transformations in Metals and Alloys, (Revised Reprint), CRC press, 2009.
[44] W. Kurz, D.J. Fisher, Fundamentals of solidification, (1989).
[45] D. Zhao, Y. Li, Lattice distortion induced site dependent carbon gettering at twin boundaries in silicon, Journal of Alloys and Compounds, 712 (2017) 599-604.
[46] D. Zhao, Y. Li, Revealing the factors influencing grain boundary segregation of P, As in Si: Insights from first-principles, Acta Materialia, 168 (2019) 52-62.
[47] M. Senechal, The genesis of growth twins, Sov. Phys. Crystallogr, 25 (1980) 520-524.
[48] R.W. Cahn, Twinned crystals, Advances in Physics, 3 (1954) 363-445.
[49] S.-Z. Lu, A. Hellawell, The mechanism of silicon modification in aluminum-silicon alloys: Impurity induced twinning, Metallurgical Transactions A, 18 (1987) 1721-1733.
[50] K. Fujiwara, K. Maeda, N. Usami, G. Sazaki, Y. Nose, K. Nakajima, Formation mechanism of parallel twins related to Si-facetted dendrite growth, Scripta Materialia, 57 (2007) 81-84.